

Supporting Information for:

The Control of Conjugation Degree via Position Engineering to Highly Efficient Phosphorescent Host Materials

Ye-Xin Zhang, Lei Zhang, Lin-Song Cui, Chun-Hong Gao, Hua Chen, Qian Li, Zuo-Quan Jiang,* and Liang-Sheng Liao*

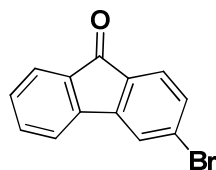
Jiangsu Key Laboratory for Carbon-Based Functional Materials & Devices, Institute of Functional Nano & Soft Materials (FUNSOM) & Collaborative Innovation Center of Suzhou Nano Science and Technology, Soochow University, Suzhou 215123, P.R. China

| | |
|---|-----|
| Table of Contents | S1 |
| Synthetic and general procedures | S2 |
| Figure S1. ¹ H NMR spectrum of 3-BrSAF. | S4 |
| Figure S2. ¹³ C NMR spectrum of 3-BrSAF. | S5 |
| Figure S3. ¹ H NMR spectrum of SAFDPA. | S5 |
| Figure S4. ¹³ C NMR spectrum of SAFDPA. | S6 |
| Figure S5. ¹ H NMR spectrum of SAFCz. | S6 |
| Figure S6. ¹³ C NMR spectrum of SAFCz. | S7 |
| Figure S7. DSC curves of SAFDPA and SAFCz. | S7 |
| Figure S8. TGA curves of SAFDPA and SAFCz. | S8 |
| Figure S9. Cyclic voltammographs of SAFDPA and SAFCz. | S8 |
| Figure S10. The spatial distribution of the lowest and highest NTOs of SAFDPA and SAFCz. | S9 |
| Figure S11. Power efficiency curves and EL spectrum of devices A and B. | S9 |
| Figure S12. Device performance of white OLEDs. | S9 |
| Figure S13. PL spectra in hexane and dichloromethane solution at 10 ⁻⁵ M. | S10 |
| Figure S14. The current density–voltage (J–V) curves for the hole-only devices (ITO/MoO ₃ (10 nm)/SAFDPA or SAFCz (100 nm)/MoO ₃ (10 nm)/Al (100 nm) | S10 |
| Figure S15. The EL spectrum of white OLED | S10 |
| Figure S16. Energy level diagrams for blue and white devices | S11 |
| Table S1. CIE under different voltage | S11 |
| Table S2. Summary of OLED Performances | S12 |

General Information: All chemicals and reagents were used as received from commercial sources without further purification. THF was purified by PURE SOLV (Innovative Technology) purification system. ^1H NMR and ^{13}C NMR spectra were recorded on a Bruker 400 spectrometer at room temperature. Mass spectra were recorded on a Thermo ISQ mass spectrometer using a direct exposure probe. UV-Vis absorption spectra were recorded on a Perkin Elmer Lambda 750 spectrophotometer. PL spectra and phosphorescent spectra were recorded on a Hitachi F-4600 fluorescence spectrophotometer. Differential scanning calorimetry (DSC) was performed on a TA DSC 2010 unit at a heating rate of $10\text{ }^\circ\text{C min}^{-1}$ under nitrogen. The glass transition temperatures (T_g) were determined from the second heating scan. Thermogravimetric analysis (TGA) was performed on a TA SDT 2960 instrument at a heating rate of $10\text{ }^\circ\text{C/min}$ under nitrogen, temperature at 5% weight loss was used as the decomposition temperature (T_d). HOMO were determined from Ultra-Violet Photoemission Spectroscopy (UPS) which made by KRATOS ANALYTICAL SHIMADZU GROUP COMPANY.

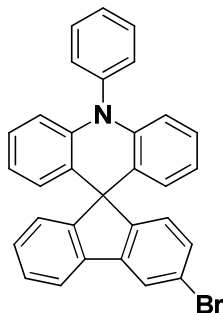
Preparation of 3-Bromofluorenone, 3-BrSAF, SAFDPA and SAFCz.

Preparation of 3-Bromofluorenone



2-amino-4-bromobenzophenone (10 g, 36.21 mmol) was stirred into 50 ml of 80% sulfuric acid at $60\text{ }^\circ\text{C}$ over half hour. The solution was cooled to $5\text{ }^\circ\text{C}$ and diazotized of sodium nitrite (2.4 g, 36.21 mmol) in 5 ml water. After 2 hours the mixture was cooled and filtered at $50\text{ }^\circ\text{C}$, resulting in 7.5 g light yellow solid (80% yield).^[1]

Preparation of 3'-bromo-10-phenyl-10H-spiro(acridine-9,9-fluorene) (3-BrSAF)

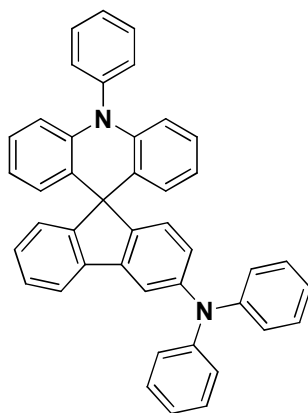


2-Bromotriphenylamine (3.24 g, 10 mmol) was dissolved in 80 mL THF in a 200 mL Schlenk tube under argon. After the solution was cooled to $-78\text{ }^\circ\text{C}$, *n*-butyl lithium (4.38 mL, 10.5 mmol) was added dropwise via a syringe. The resulting mixture was allowed to stir for 1 hour at $-78\text{ }^\circ\text{C}$, and then 3-bromofluorenone (3.38 g, 10 mL) in 80 mL THF was added over a period of 0.5 hour. After 1 hour

reaction at $-78\text{ }^{\circ}\text{C}$, the mixture was gradually warmed up to room temperature overnight. 5 mL water was added to the mixture and THF was evaporated under reduced pressure. The resulting solid was dissolved in 80 mL dichloromethane and washed with water (3 x 50 mL). Then the organic layer was separated, dried over sodium sulfate, filtered and evaporated, resulting in 4.51 g light yellow solid, which was directly used in the next reaction without further purification.

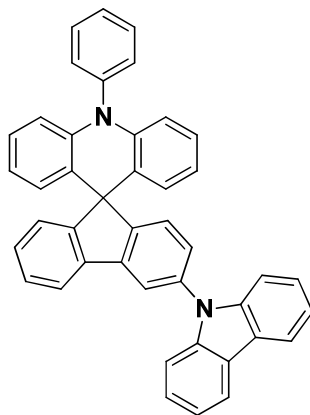
The crude product was dissolved in 45 mL acetic acid and 4.5 mL hydrochloric acid (36%). After refluxed for 4 hours under stirring, the reaction was cooled to room temperature, filtered and washed with petroleum ether. The resulting solid was further purified by column chromatography using petroleum ether as eluent to afford a white powder (4.06 g, 83.4%). ^1H NMR (400 MHz, CDCl_3): δ = 6.34-6.40 (m, 4H), 6.55-6.59 (m, 2H), 6.90-6.94 (m, 2H), 7.27-7.30 (m, 2H), 7.35-7.44 (m, 3H), 7.47-7.49 (m, 2H), 7.55-7.59 (m, 1H), 7.69-7.76 (m, 3H), 7.92 (d, J = 1.6 Hz, 1H) ppm. ^{13}C NMR (100 MHz, CDCl_3): δ = 156.77, 155.34, 141.38, 141.22, 140.92, 137.89, 131.12, 131.10, 129.13, 128.52, 127.78, 127.61, 127.40, 127.28, 125.93, 123.96, 123.12, 121.64, 120.60, 120.13, 114.75, 56.61 ppm. MS m/z : 485.22. Anal. calcd for $\text{C}_{31}\text{H}_{20}\text{BrN}$ (%): C 76.55, H 4.14, N 2.88; found: C 76.38, H 4.28, N 3.92.

Preparation of N,N' -10-triphenyl-10H-spiro(acridine-9,9-fluorene)-3'-amine (SAFDPA)



3-BrSAF (2.43 g, 5.0 mmol), diphenylamine (1.27 g, 7.5 mmol), palladium acetate (0.022 g, 0.1 mmol), tri-*t*-butylphosphonium tetrafluoroborate (0.087 g, 0.3 mmol), sodium *t*-butoxide (1.20 g, 12.5 mmol) were dissolved in toluene under argon. After refluxed for 10 hours under stirring, the reaction was cooled to room temperature and 50 mL water was added. The organic layer was separated and the aqueous layer was extracted with 15 mL toluene twice. Then the extracts were combined, dried over sodium sulfate, filtered and evaporated under reduced pressure. The crude product was purified by column chromatography using petroleum ether/dichloromethane (2/1, v/v) as eluent to afford final product. The final product was a white crystalline powder (2.59 g, 90.0%). ^1H NMR (400 MHz, CDCl_3): δ = 6.35-6.37 (m, 2H), 6.51-6.53 (m, 2H), 6.60-6.64 (m, 2H), 6.91-6.97 (m, 3H), 7.02 (t, J = 7.3 Hz, 2H), 7.14-7.16 (m, 4H), 7.23-7.33 (m, 7H), 7.42-7.50 (m, 4H), 7.56 (t, J = 7.6 Hz, 1H), 7.61 (d, J = 7.2 Hz, 1H), 7.67-7.71 (m, 2H) ppm. ^{13}C NMR (100 MHz, CDCl_3): δ = 156.69, 150.95, 147.95, 147.47, 141.38, 141.04, 140.21, 139.12, 131.16, 131.04, 129.26, 128.43, 128.38, 127.62, 127.47, 127.14, 126.14, 125.80, 125.09, 124.57, 124.25, 122.69, 120.51, 119.97, 115.31, 114.59, 56.44 ppm. MS m/z : 574.28. Anal. calcd for $\text{C}_{43}\text{H}_{30}\text{N}_2$ (%): C 89.86, H 5.26, N 4.87; found: C 89.78.38, H 5.38, N 4.83.

Preparation of 3'-(9H-carbazol-9-yl)-10-phenyl-10H-spiro(acridine-9,9-fluorene) (SAFCz)



3-BrSAF (2.43 g, 5.0 mmol), carbazole (1.25 g, 7.5 mmol), Pd₂(dba)₃ (0.092 g, 0.1 mmol), tri-*t*-butylphosphonium tetrafluoroborate (0.029 g, 0.1 mmol), sodium *t*-butoxide (1.20 g, 12.5 mmol) were dissolved in toluene under argon. After refluxed for 10 hours under stirring, the reaction was cooled to room temperature and 50 mL water was added. The organic layer was separated and the aqueous layer was extracted with 15 mL toluene twice. Then the extracts were combined, dried over sodium sulfate, filtered and evaporated under reduced pressure. The crude product was purified by column chromatography using petroleum ether/dichloromethane (2/1, v/v) as eluent to afford final product. The final product was a white crystalline powder (2.73, 95.5%).

¹H NMR (400 MHz, CDCl₃): δ = 6.40-6.43 (m, 2H), 6.55-6.57 (m, 2H), 6.64-6.68 (m, 2H), 6.96-7.00 (m, 2H), 7.27-7.35 (m, 3H), 7.38-7.44 (m, 4H), 7.50-7.54 (m, 5H), 7.58 (dd, *J* = 7.6 Hz, 1H), 7.64-7.78 (m, 4H), 7.95 (d, *J* = 1.6 Hz, 1H), 8.16 (d, *J* = 7.6 Hz, 2H) ppm. ¹³C NMR (100 MHz, CDCl₃): δ = 156.56, 155.58, 141.40, 140.99, 140.96, 140.67, 138.79, 137.19, 131.14, 131.12, 129.06, 128.54, 127.49, 126.80, 125.91, 124.41, 123.36, 120.30, 120.18, 119.90, 118.49, 114.80, 109.98, 56.89 ppm. MS *m/z*: 572.31. Anal. calcd for C₄₃H₂₈N₂ (%): C 90.18, H 4.93, N 4.89; found: C 89.98.38, H 5.17, N 4.84.

Fabrication of OLEDs: The OLEDs were fabricated by vacuum deposition onto ITO-coated glass substrates with a resistance of ca. 30 Ω per square. The ITO surface was cleaned with acetone, ethanol, and deionized water, then dried in an oven, and finally exposed to UV-ozone for about 30 min. Organic materials were deposited at a rate of 2-3 Å/s and Liq was deposited at 0.2 4 Å/s then capped with Al (ca. 4 Å/s) through a shadow mask without breaking the vacuum. For the EL spectra, CIE coordinates and J-V-L curves of the devices, all of them were measured with a PHOTO RESEARCH SpectraScan PR 655 photometer and a KEITHLEY 2400 SourceMeter constant current source at room temperature.

Figure S1. ¹H NMR spectrum of 3-BrSAF

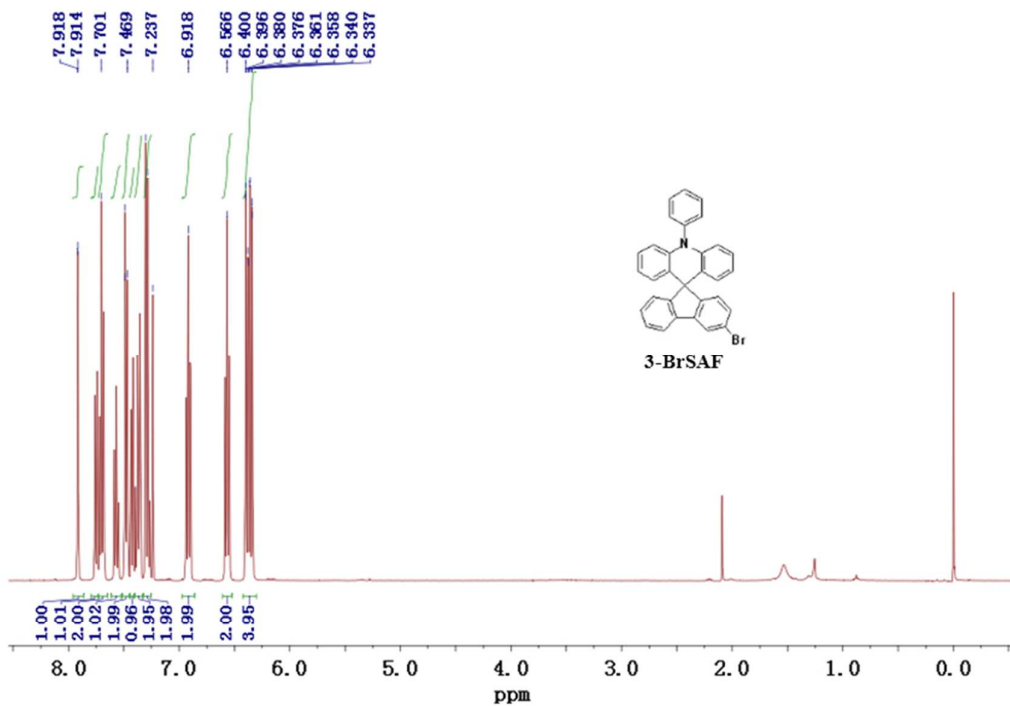


Figure S2. ^{13}C NMR spectrum of 3-BrSAF.

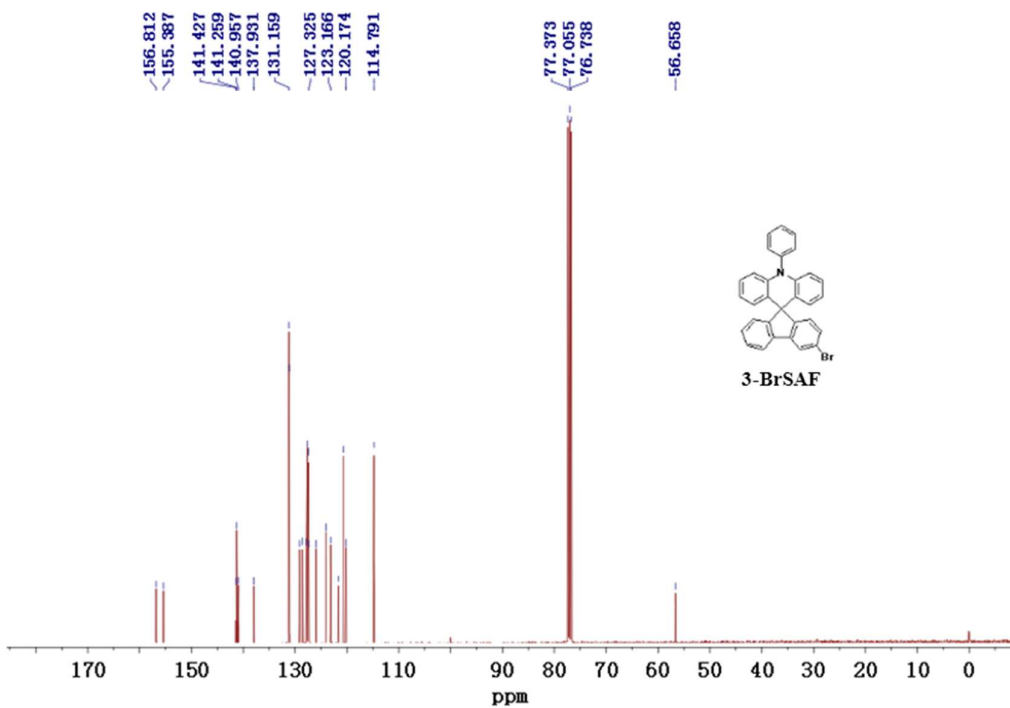


Figure S3. ^1H NMR spectrum of SAFDPA.

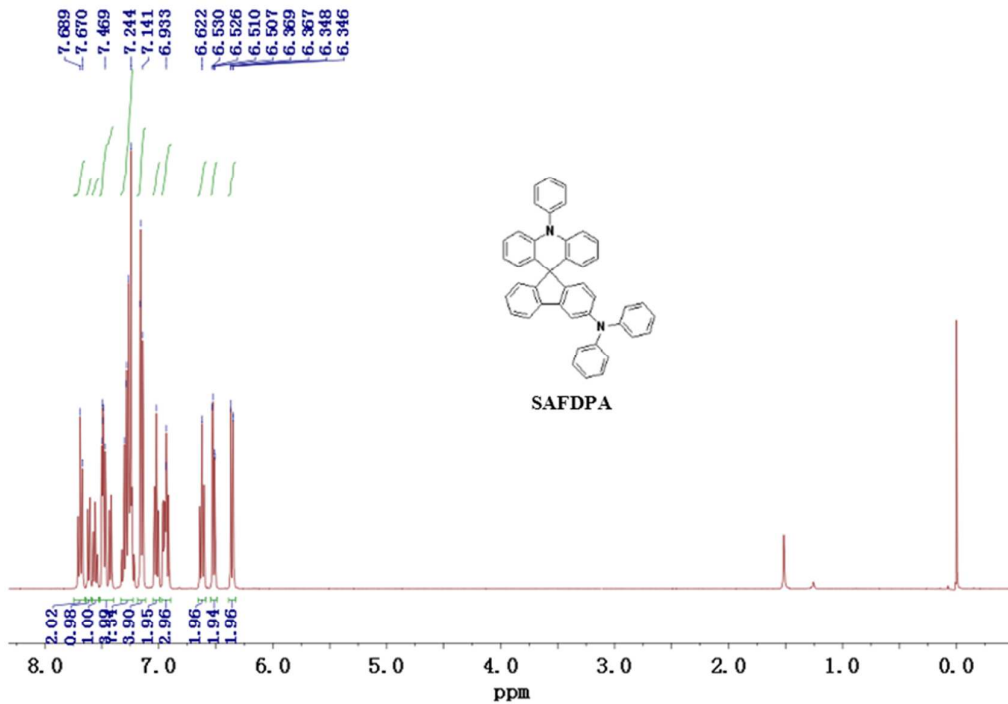


Figure S4. ^{13}C NMR spectrum of SAFDPA.

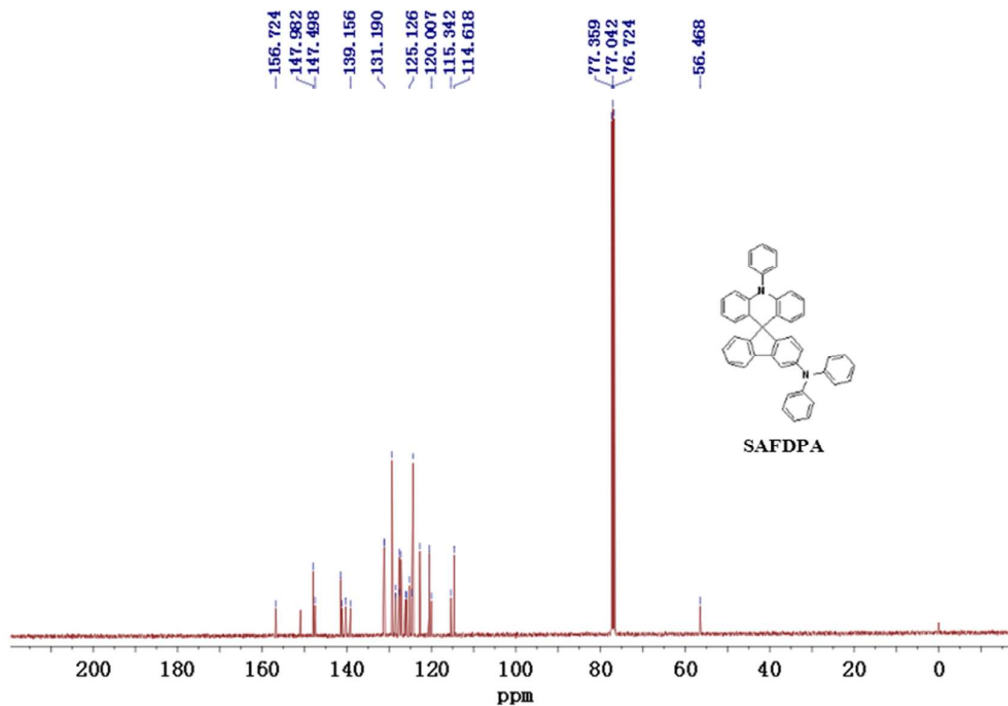


Figure S5. ^1H NMR spectrum of SAFDPA.

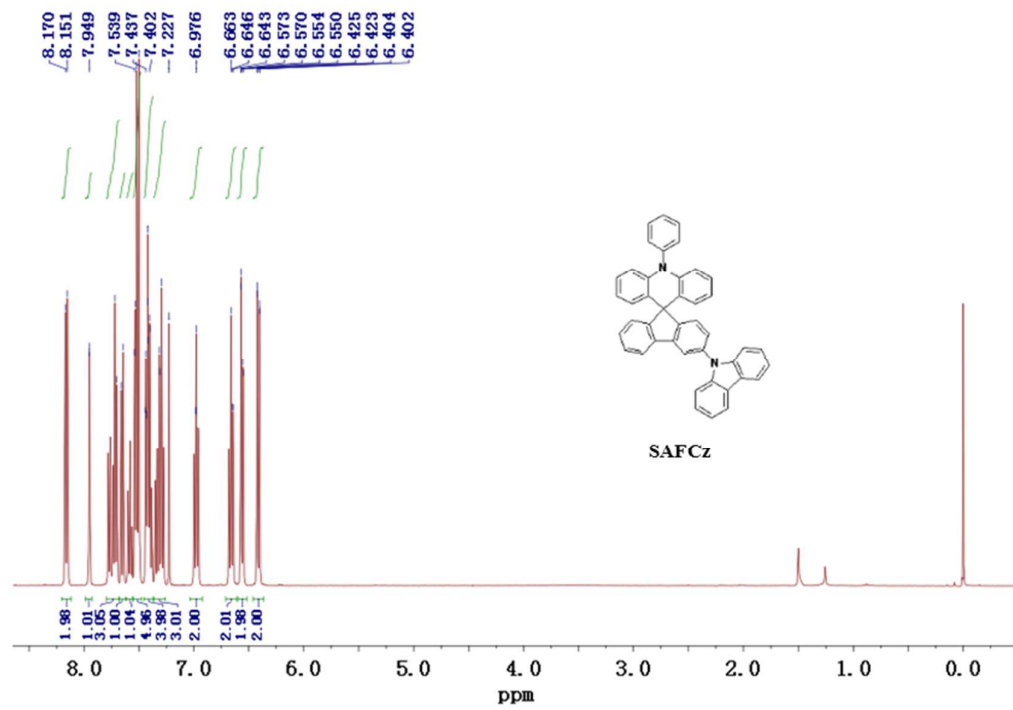


Figure S6. ^{13}C NMR spectrum of SAFCz.

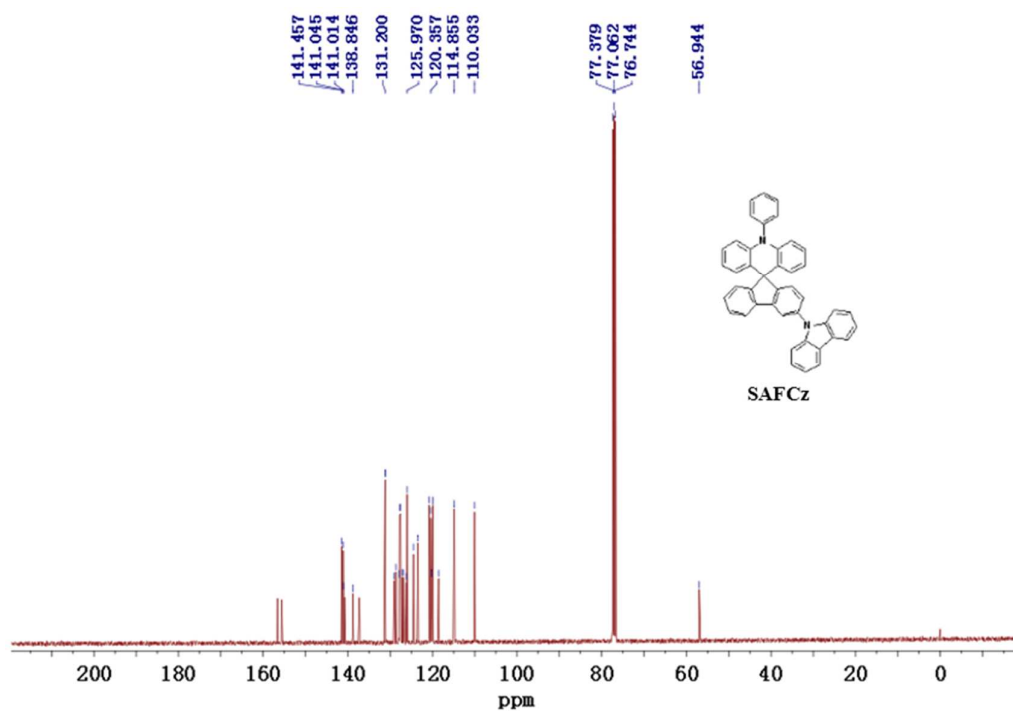


Figure S7. DSC traces recorded at a heating rate of $10\text{ }^{\circ}\text{C}/\text{min}$

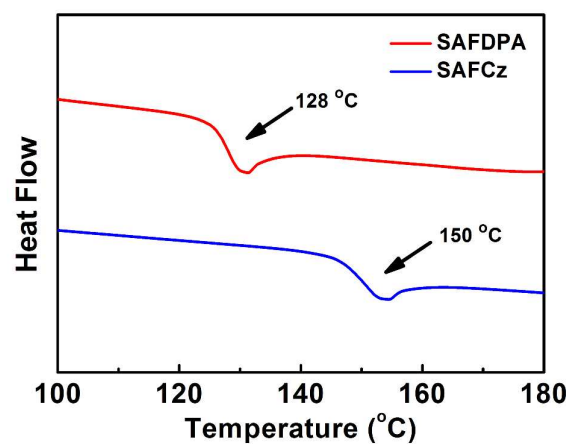


Figure S8. TGA traces recorded at a heating rate of 10 °C/min.

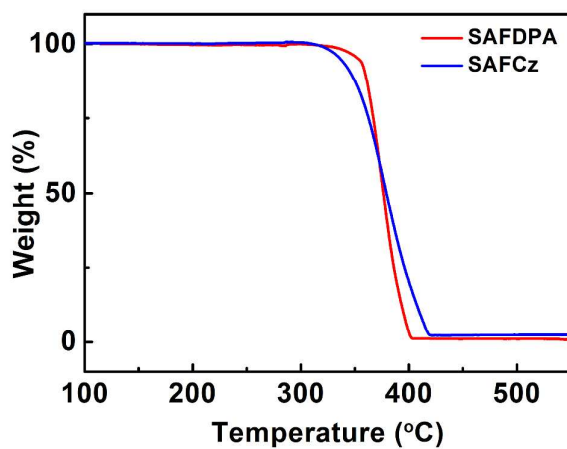


Figure S9. Cyclic voltammograms of SAFDPA and SAFCz in dichloromethane solution for oxidation

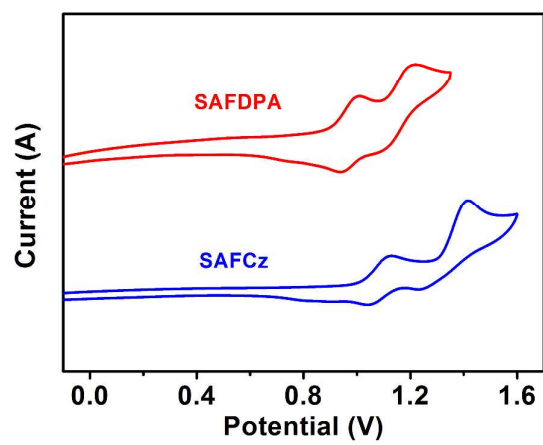


Figure S10. The spatial distribution of the lowest and highest NTOs of SAFDPA and SAFCz

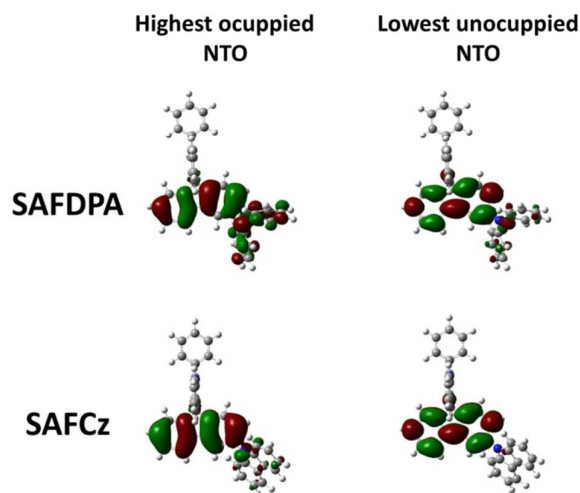


Figure S11. (a) Power efficiency curves; (b) The EL spectrum of devices A and B at 10 mA/cm².

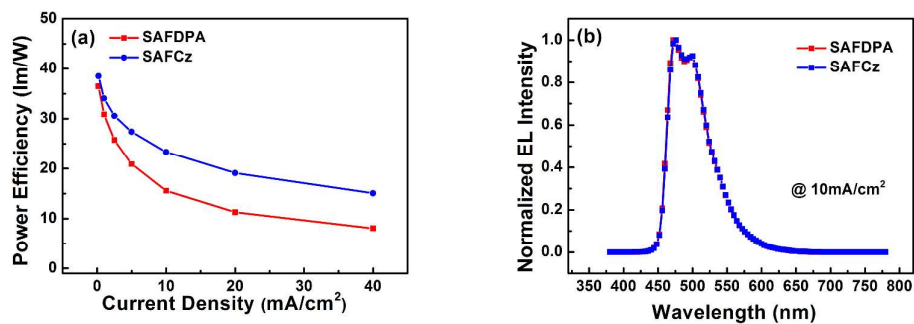
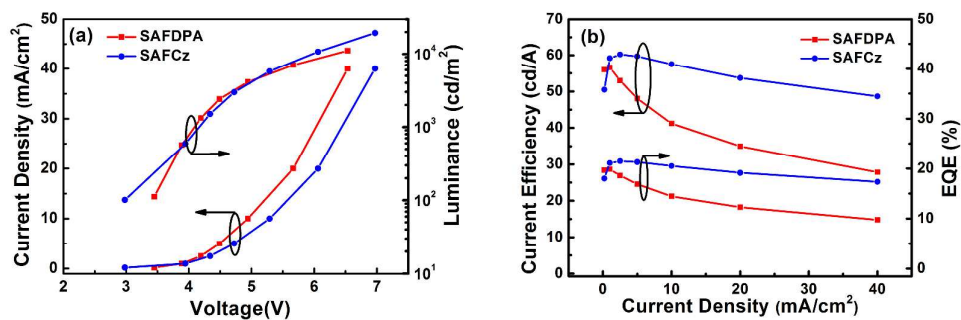


Figure S12. (a) Current density-voltage-luminance characteristics; (b) External quantum efficiency versus current density curves; (c) Power efficiency curves; (d) The EL spectrum of devices A and B at 10 mA/cm².



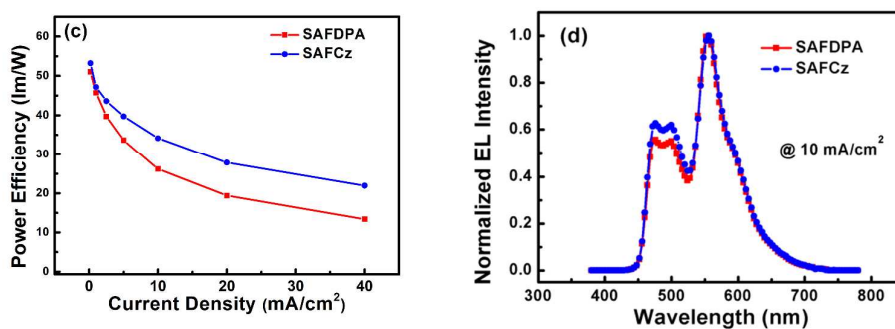
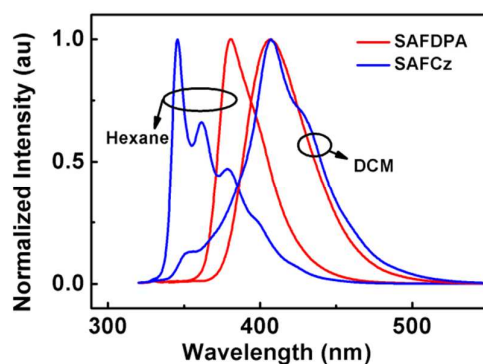


Figure S13. PL spectra in hexane and dichloromethane solution at 10^{-5} M.



Due to the HOMO (triphenylamine) and LUMO (fluorene) is perpendicular to each other in SAFCz, the transition between HOMO and LUMO is forbidden. Thus, we observed a PL emission originated the LE state on fluorene part. For SAFDPA, there is an overlap zone for HOMO and LUMO, which means the CT state is easier to be formed. Along with the increase the polarity of solvent, the CT state in SAFCz is stabilized and its energy decreases. Hence, we can observe the structureless PL spectrum. These phenomena are in consistent with the frontier orbitals distribution in the manuscript.

Figure S14. The current density–voltage (J–V) curves for the hole-only devices (ITO/MoO₃ (10 nm)/SAFDPA or SAFCz (100 nm)/MoO₃ (10 nm)/Al (100 nm)).

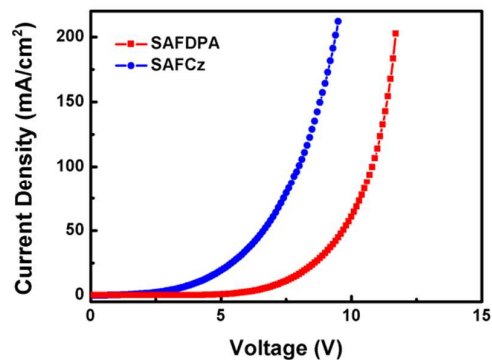


Figure S15. The EL spectrum of white OLED.

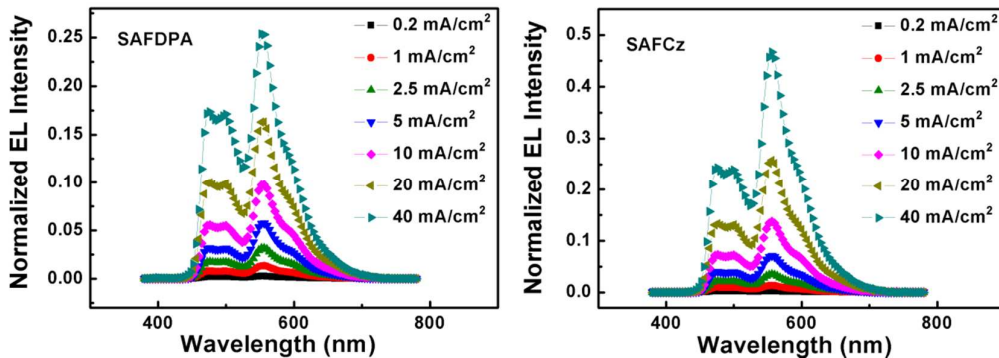
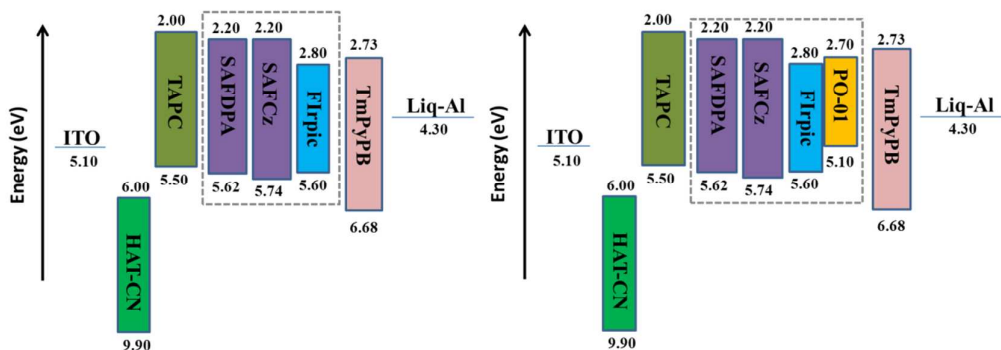


Figure S16. Energy level diagrams for blue and white devices



The device performance results with SAFCz are a bit better than that of SAFDPA (we could consider both materials showed comparable max. efficiencies). It could be attributed the different HOMO energy levels of the host materials. SAFCz (-5.74 eV) is 0.14 eV deeper than SAFDPA (-5.62 eV) in HOMO level. In common devices, holes are surplus. Materials with deeper HOMO level could block redundant holes, as a result, it could improve charge balance in emissive layer.

Table S1. CIE under different voltage

| | Voltage (V) | CIE _(x,y) | | Voltage (V) | CIE _(x,y) |
|------|-------------|----------------------|------|--------------|----------------------|
| | SAFDPA | 3.44 | | (0.32,0.47) | SAFCz |
| 3.88 | | (0.34,0.48) | 3.94 | (0.33,0.47) | |
| 4.19 | | (0.35,0.48) | 4.33 | (0.34,0.47) | |
| 4.48 | | (0.35, 0.48) | 4.72 | (0.35, 0.48) | |
| 4.94 | | (0.35, 0.48) | 5.28 | (0.36, 0.48) | |
| 5.66 | | (0.34, 0.47) | 6.06 | (0.36, 0.48) | |
| 6.53 | | (0.33, 0.47) | 6.96 | (0.36, 0.48) | |

Table S2. Summary of OLED Performances

| Device | Host/ guest | At 100 cd/m ² | | At 1000 cd/m ² | | $\eta_{c,max}/\eta_{p,max}/\eta_{ext,max}^b$ (cd/A/ lm/W/ %/ V) | CIE(x,y) ^c |
|--------|-------------|--|---------------------|--|-------------|--|-----------------------|
| | | $\eta_c/\eta_p/\eta_{ext}/V^a$ (cd/A/ lm/W/ %/ V) | | $\eta_c/\eta_p/\eta_{ext}/V^a$ (cd/A/ lm/W/ %/ V) | | | |
| A | SAFDPA/ B | 39.0/36.5/16.3/3.4 | 34.4/ 25.7/14.4/4.2 | 39.0/36.5/16.3/3.4 | (0.16,0.38) | | |
| B | SAFCz/ B | 41.5/38.5/17.3/3.4 | 41.6/30.6/17.4/4.3 | 42.1/38.5/17.4/3.4 | (0.16,0.38) | | |
| C | SAFDPA/B+Y | 56.0/51.0/17.8/3.4 | 56.6/45.7/16.9/3.9 | 56.6/51.0/18.0/3.4 | (0.35,0.48) | | |
| D | SAFCz/ B+Y | 50.5/53.2/16.3/3.0 | 60.2/43.6/19.5/4.3 | 60.2/53.2/19.5/3.0 | (0.33,0.47) | | |

^a Current efficiency (η_c), power efficiency (η_p), external quantum efficiency (η_{ext}), voltage (V) at 100 cd/m² and 1000 cd/m². ^b Maximum current efficiency ($\eta_{c,max}$), maximum power efficiency ($\eta_{p,max}$), maximum external quantum efficiency ($\eta_{ext,max}$). ^c Measured at 10 mA/cm².

Reference

[1] Cui, L. -S.; Dong, S. -C.; Liu, Y.; Xu, M. F.; Li, Q.; Jiang, Z. -Q.; Liao, L. -S. *Org. Electron.* **2013**, 14, 1924.